Biomaterials 35 (2014) 2218–2226

Contents lists available at ScienceDirect

Biomaterials

journal homepage: www.elsevier.com/locate/biomaterials

A multi-modality platform to image stem cell graft survival in the naïve and stroke-damaged mouse brain

Philipp Boehm-Sturm [a,1], Markus Aswendt [a,1], Anuka Minassian [a], Stefanie Michalk [a], Luam Mengler [a], Joanna Adamczak [a], Laura Mezzanotte [b], Clemens Löwik [b], Mathias Hoehn [a,b,*]

[a] In-Vivo-NMR Laboratory, Max-Planck-Institute for Neurological Research in Cologne, Cologne, Germany
[b] Department of Radiology, Leiden University Medical Center, Leiden, The Netherlands

ARTICLE INFO

Article history:
Received 6 November 2013
Accepted 27 November 2013
Available online 17 December 2013

Keywords:
Neural stem cells
19F-MRI
BLI
Stroke
MCAO
Stem cell implantation

ABSTRACT

Neural stem cell implantations have been extensively investigated for treatment of brain diseases such as stroke. In order to follow the localization and functional status of cells after implantation noninvasive imaging is essential. Therefore, we developed a comprehensive multi-modality platform for *in vivo* imaging of graft localization, density, and survival using 19F magnetic resonance imaging in combination with bioluminescence imaging. We quantitatively analyzed cell graft survival over the first 4 weeks after transplantation in both healthy and stroke-damaged mouse brain and correlated our findings of graft vitality with the host innate immune response. The multi-modality imaging platform will help to improve cell therapy also in context other than stroke and to gain indispensable information for clinical translation.

1. Introduction

Transplantation of stem cells is an appealing strategy for a more efficient treatment of stroke since the disease leads to widespread, irreversible cell loss. Neural stem cells (NSCs) are of particular interest for therapy since they can differentiate into all neural cell types without tumorigenic potential. NSCs isolated from embryonic, fetal and adult mammalian tissue and derived from embryonic or induced-pluripotent stem cells have been used in experimental stroke therapy [1,2]. Functional recovery was associated to some extent with NSC migration and integration. Furthermore, modulation of inflammation, angiogenesis, cell death, and plasticity have been described [2]. However, before stem cells can be used for the treatment of patients, the timing, route of delivery, implantation site, and dosage need to be optimized in animal studies [3]. To this end, noninvasive imaging provides information about the spatio-temporal dynamics of cells after transplantation and ideally about their functional state. Thus far, the imaging modality of choice to study cell migration in deep tissues with high resolution is 1H magnetic resonance imaging (MRI) of cells that have been pre-labeled with superparamagnetic iron oxide (SPIO) particles [4]. However, the contrast generated by SPIO-labeled cells is ambiguous against non-homogenous background tissue and cell quantification is extremely difficult. Recently, we and others demonstrated NSC imaging using perfluorocarbon (PFC)-based cell labels, which are detectable via fluorine magnetic resonance imaging (19F-MRI) [5–7]. 19F-MRI provides highly specific information on the localization of cells due to absence of 19F in biological tissue. Moreover, it allows quantification of cell numbers *in vivo* [8]. However, both SPIO- and PFC-based MRI do not provide information on cell viability or functionality. In recent studies, this was overcome by combining SPIO labels with a genetic “label”, the luciferase gene [9–11]. Luciferases, in the presence of their substrate, generate a natural form of chemiluminescence called bioluminescence. The luciferase gene can be expressed in mammalian cells, which allows the tracking of genetically modified cells in the living animal quantitatively and noninvasively by bioluminescence imaging (BLI). Since the light is generated from within the living animal and there is no endogenous background signal, BLI is very sensitive. For the experiments reported here, a

* Corresponding author. In-Vivo-NMR Laboratory, Max Planck Institute for Neurological Research, Gleuelerstrasse 50, D-50931 Cologne, Germany. Tel.: +49 221 4726 315/336; fax: +49 221 4726 337.
E-mail address: mathias@nf.mpg.de (M. Hoehn).
[1] These authors contributed equally to this work.

0142-9612
http://dx.doi.org/10.1016/j.biomaterials.2013.11.085

modified click beetle luciferase (CBG99) was used, which emits light at 543 nm and is particularly favorable for *in vivo* BLI due to its high quantum yield [12].

In previous invasive experiments, a large fraction of cells was reported to die after implantation to the brain [13–15] and the number of surviving cells could not be improved by implanting more cells in a model of stroke [16]. Exact mechanisms and the temporal profile of this cell loss are largely unknown since invasive studies provide only snapshot data from single animals. The rejection by the host innate immune system is thought to be a key player particularly in allogeneic and xenogeneic grafts [17,18]. Interestingly, global cerebral ischemia transiently enhances NSC graft survival in immunocompetent mice [19] indicating that the balance between trophic and inflammatory signals is shifted toward improved cell viability.

Since similar cues associated with neuroinflammation may also be active after focal cerebral ischemia and direct comparison of NSC graft survival in healthy and stroke-damaged tissue is still pending, we developed a quantitative framework to assess transplanted stem cell graft localization and survival *in vivo* using 19F-MRI and BLI. To lower the risk of rejection and in order to focus on the impact of the innate immune system on graft survival we used T-lymphocyte deficient Nu/Nu mice. Using our newly developed 19F-MRI-optical imaging platform in mice that received an NSC implant after focal cerebral ischemia we aimed to i) follow the spatio-temporal dynamics of NSCs in a quantitative manner (19F-MRI) and assess graft survival (BLI), ii) compare survival of NSCs in the naïve and stroke-damaged brain (BLI) and iii) correlate graft survival with the innate immune system response using antibody staining of activated microglia and astrocytes.

2. Materials and methods

2.1. Study design

NMRI-Foxn1nu/Foxn1nu mice (age 8–10 weeks, 25–30 g, male from Janvier, Saint Berthevin Cedex, France) were divided into the following groups: naïve mice that received implantations of multi-labeled NSCs ($n = 7$), pure 19F agent ($n = 3$), nonlabeled NSCs ($n = 12$), or HBSS ($n = 3$) and mice that underwent middle cerebral artery occlusion (MCAO) and received implantation of multi-labeled NSCs ($n = 4$). Animals underwent sequential BLI and MRI up to four weeks. All experiments were conducted according to the guidelines laid out in the German Animal Welfare Act and approved by the local authorities. Numbers represent final numbers after exclusion of animals that did not show significant signal in one of the imaging modalities at the first imaging session. Stroke animals that did not have a lesion on T2-weighted MR images 24 h after surgery or that lost more than 20% bodyweight were also excluded. These criteria were agreed on before the study. One stroke animal was excluded retrospectively since 19F MR images showed strong signal from directly underneath the skin. This indicated a failed transplantation during which cells were pushed back through the injection canal. Replicates are indicated throughout the text and were always true experimental replicates.

2.2. Generation of cell line

Radial glia-like NSCs were derived from the murine embryonic stem cell line CGR8 (generous gift from Prof. A. Sachinidis, Institute for Neurophysiology, University at Cologne, Germany) by adaption of existing protocols [20,21]. The click beetle luciferase CBG99 from pGL3-CBG99 (Promega, Madison, USA) was cloned into the multiple cloning site (MCS) of the lentiviral expression vector pRLL-PGK [22] (kind gift of Prof. Hoeben, Leiden University Medical Center, Leiden, The Netherlands) by the restriction enzymes NheI and XbaI. N2EuroCBG99 cells were generated by lentiviral-vector mediated transduction [22]. For detailed description see Supplementary materials and methods.

A gene marker profile analysis via reverse transcription polymerase chain reaction (RT-PCR) of 20 genes was performed. For the complete protocol and list of primer pairs (Table S1) see Supplementary materials and methods.

2.3. Cell labeling

Cells were seeded (63,000 cells/cm^2) 4 h before labeling on 6-well plates (Greiner Bio-One, Germany). A PFC nanoemulsion with or without fluorescence label (CS-1000 or CS green, Celsense Inc., Pittsburgh, USA) was added at 25 μl/ml for 42 h. A subgroup of 19F-labeled cells received an additional permanent, intracellular fluorescence label (CellTracker Orange – CTO, Life Technologies, Carlsbad, USA) according to the manufacturer's protocol. (Multi-)Labeled cells and unlabeled control cells were harvested with Accutase (PAA Laboratories GmbH, Cölbe, Germany) and centrifuged at 250 × g for 3 min, washed 3× with PBS (PAA) to remove label excess and counted by the trypan blue exclusion method to determine the viable/dead ratio. For further experiments the labeled cells were subsequently prepared in one of the following ways: i) dissolved in HBSS (Life Technologies) for transplantation (150,000 cells/μl), ii) fixed with paraformaldehyde (PFA) to determine 19F/cell with MR spectroscopy as previously described [6], or iii) plated for cell characterization.

2.4. Characterization of multi-labeled NSCs

To assess possible adverse effects of the multi-labeling on cell function, we performed extensive *in vitro* tests of viability, migration, proliferation, differentiation, and luciferase expression on single-labeled (19F or CTO) and multi-labeled (19F and CTO) CBG99 + NSCs. Wildtype (WT) and unlabeled cells served as controls. These assays are described in Supplementary materials and methods.

2.5. Middle cerebral artery occlusion

Focal cerebral ischemia was induced using the filament model as described by Bahmani et al. [23]. Briefly, mice were anesthetized with 1–2% isoflurane in a O2/N2O (30:70%) and received a subcutaneous (s.c.) injection of 4 mg/kg buprenorphin (Temgesic, Merck, Darmstadt, Germany) for analgesia. A silicon rubber-coated filament with a tip diameter of 170 μm (Doccol Corporation, Sharon, MA USA) was used to block the blood flow to the middle cerebral artery (MCA). Animals were allowed to recover during the 30 min occlusion and subsequently reanesthetized to initiate reperfusion by filament removal. The common carotid artery (CCA) was permanently ligated. 24 h after MCAO, animals were scanned with T2-weighted MRI in order to delineate the lesion and to determine stereotactic coordinates for peri-infarct implantations at 48 h post stroke.

2.6. Cell implantation

Implantation as described in detail elsewhere [24] was applied 48 h after MCAO. T2-weighted MRI of the peri-infarct zone 24 h after MCAO was used to determine implantation coordinates. Briefly, mice were anesthetized with Isoflurane in O2:N2O (30:70%), and 4 mg/kg Carprofen (Pfizer, Berlin, Germany) was injected s.c. for analgesia. During surgery, mice remained fixed in a stereotactic frame (Stoelting, Dublin, Ireland). For all naïve and stroke animals, the following coordinates relative to bregma were selected using a stereotactic instrument (Stoeltin): AP +0.5; L +2.0; DV −3.0. 300,000 NSCs were injected into the brain through a Hamilton syringe (26G needle) using a micropump system.

2.7. Bioluminescence imaging

Animals were anesthetized with 2% Isoflurane in 100% O_2, injected with 150 mg/kg D-Luciferin sodium (Synchem, Felsberg, Germany) i.p. and placed on a custom-made holder with two side view mirrors. The time lag between substrate injection and acquisition was recorded for each experiment and used for time-line correction. Bioluminescence data was acquired in list mode for 30 min with the Photon Imager (Biospace Lab, Paris, France) and analyzed by calculations on dynamic time curves with 5 and 60 s temporal resolution [25]. BLI signal change is expressed in % in relation to the data from the first week (day 1 or 7) after transplantation. For multimodal imaging experiments, animals were allowed to recover for at least 6 h before 19F-MRI to ensure wash-out of Isoflurane from the earlier BLI experiment.

2.8. Magnetic resonance imaging

MRI was carried out on a Biospec 11.7 T animal scanner system (Bruker BioSpin, Ettlingen, Germany). For radiofrequency transmission and reception, we used a custom-built, inductively coupled, single-loop surface coil of 20 mm, tunable from 470 MHz for 19F up to 500 MHz for 1H. Anesthesia was initiated using Ketamine/Xylazine (100 mg kg^{-1}/10 mg kg^{-1} i.p.) and prolonged after 40 min by Ketamine (25 mg kg^{-1} s.c. every 15 min). Respiration rate was monitored using a pressure sensitive pad placed under the thorax, body temperature was maintained at 37 °C with an in-house feedback-controlled system, and 100% oxygen was delivered through a nose cone. Animals were fixed with ear bars in standard animal holders (Bruker BioSpin). Anatomical 1H MRI was performed with a turbo spin echo sequence (repetition time/effective echo time = 2.2 s/42.8 ms, 8 echoes per excitation, number of averages = 4, 20 consecutive, coronal, 0.5 mm thick slices, field of view = 2.28 * 1.92 cm^2, 192 * 128 matrix, acquisition time = 2:21 min, bandwidth = 50 kHz). 19F images were acquired with the same sequence and matching geometry but slightly different parameters: effective echo time = 10.5 ms, number of averages = 256, 10 consecutive, 1 mm thick slices, 72 * 48 matrix, BW = 15 kHz, TA = 56:19 min). The imaging session did not exceed 1.5 h. Total integrated 19F signal-to-noise ratio (SNR) of each graft was analyzed as described previously [6]. To study NSC migration, images were registered with an affine transformation to a template mouse brain (average of high resolution T2-weighted MR images from 6 Nu/Nu mice) using FMRIB Software Library (http://www.fmrib.ox.ac.uk/fsl/).

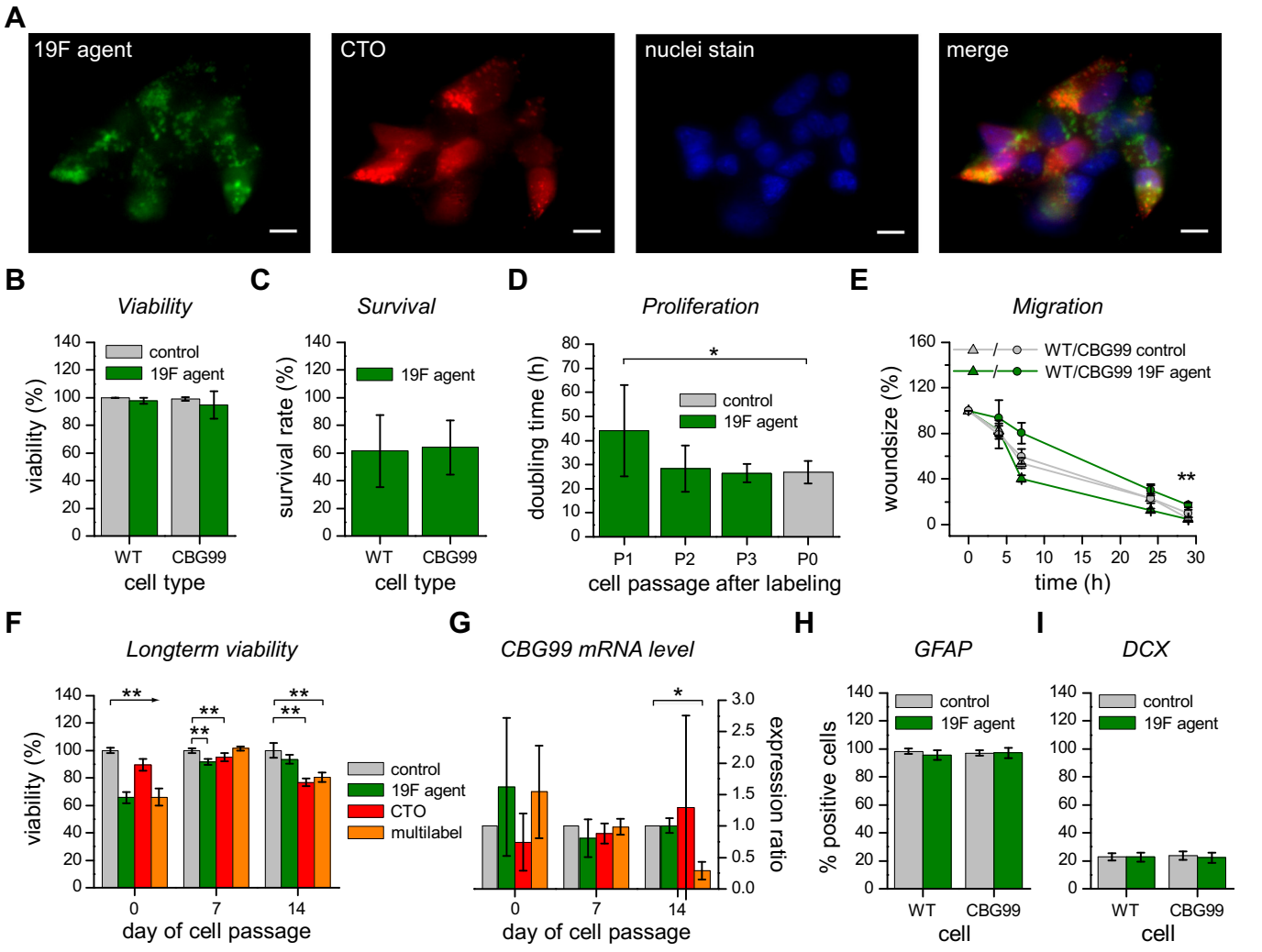

Fig. 1. *In vitro* characterization of multi-labeled cells. (A) Fluorescence images of multi-labeled cells counterstained with Hoechst show colocalization of 19F agent CS-green and CellTracker Orange (CTO) in the cytoplasm. Scale bar represents 10 μm (B–C) Trypan blue exclusion assay showed no effect on cell viability but reduced survival rate of cells labeled with the 19F agent in relation to unlabeled control. (D) Directly after 19F labeling, CBG99 cell proliferation was significantly reduced compared to control cells before labeling. (E) Migration assessed via scratch assay was similar for all cell types and labeling conditions. Only for CBG99 cells a slight effect of 19F labeling on wound size after 28 h was found. (F) Highly sensitive PrestoBlue cell viability assay showed a long-term effect of the 19F agent, CTO, and the multi-label on cell viability at 14 days. (G) The impact of the single- and multi-labeling on CBG99 mRNA level was validated by qPCR. Only the combination of both labels induced a reduction of CBG99 transcription in cells passaged for 14 days. (H) Glial (GFAP+) and neuronal (DCX+) differentiation potential was not affected by the 19F agent. */**: Significance level $p \leq 0.05/0.01$, all values presented as mean ± standard deviation.

2.9. Histology

Cells were fixed with 4% PFA before immunocytochemistry (ICC), which was performed as described in detail elsewhere [24]. Antibodies are listed in Table S2. The nuclei were counterstained by Hoechst 33342 (Sigma–Aldrich) and the cells finally mounted within Aquamount (Life Technologies). ICC was visualized under a 40× objective on a fluorescence microscope (Keyence, Neu-Isenburg, Germany) and analyzed with ImageJ. Doublecortin (DCX) and glial fibrillary acidic protein (GFAP) positive cells were quantified by counting cells manually on 5 randomly chosen fields of view.

For immunohistochemistry (IHC), mice were perfused transcardially under Isoflurane anesthesia with saline followed by 4% PFA. The brains were removed and freshly frozen in −40 °C cold 2-methylbutane and stored at −80 °C. 10–14 μm thick sections were cut in the coronal plane using a cryostat (Leica, Wetzlar, Germany). IHC was performed on the basis of a previously described protocol [14]. Antibodies are listed in Table S2. For Iba1, Ki67 antigen retrieval with 10 mM citrate buffer and fixation in acetone was applied. For Iba1 staining, HRP-DAB detection was used by applying a secondary antibody coupled to horseradish peroxidase (HRP) and 3,3′ diaminobenzidine tetrahydrochloride (DAB).

2.10. Statistics

All statistical analyses were carried out in SPSS (Version 20, IBM SPSS statistics, Ehningen, Germany). For longitudinal investigations repeated measures ANOVA was used followed by post hoc pairwise comparison with Bonferroni correction. For single time point experiments a Student's *t*-test was used for the comparison of experimental groups. A *p*-value ≤0.05 was considered to be significant. qPCR results were statistically analyzed with REST calculation as previously described [24]. All values are expressed as mean ± standard deviation.

3. Results

3.1. Generation and in vitro characterization of multi-labeled NSCs

The stable proliferating murine NSC line derived from embryonic stem cells was previously characterized as radial glia-like [21]. In agreement, we confirmed that NSCs are BLBP+/GFAP− and show an NSC expression pattern with Nestin+/Sox1−/Sox2+/Musashi1+/Prominin-1+. In addition, the oligodendrogenic marker Olig2 and GalC are present. Contamination with pluripotent (Oct4+/Nanog+/5T4−), mesodermal (Brachyury+) and endodermal (Gata6+) cells was excluded. The cells can be differentiated into neurons and glia, shown by the onset of DCX and GFAP expression and corresponding immuno-stainings (Fig. S1A, C).

For *in vivo* imaging NSCs were transduced with a lentiviral-vector to constitutively express the CBG99 luciferase (Fig. S1B). Cells were incubated with a 19F agent consisting of a PFC emulsion and additionally labeled with the permanent intracellular fluorescent probe CTO. Fluorescence microscopy revealed intracellular uptake of these markers (Fig. 1A).

To assess possible adverse effects of the multi-labeling on cell function, we performed extensive *in vitro* tests. CBG99 expression and 19F labeling had no effect on viability as measured with Trypan blue assay (Fig. 1B). However, after incubation with the 19F label, the survival rate decreased to 61.4% ± 26.2% (WT) and 64.1% ± 19.6% (CBG99) compared to unlabeled controls (Fig. 1C), which could be attributed to a significantly increased doubling time of 44.0 h ± 11.0 h compared to 26.8 h ± 1.5 h for unlabeled CBG99 cells (Fig. 1D, *t*-test, $t(10) = -2.684$, $p = 0.023$). However, this slowing of proliferation by the 19F label normalized after one passage. Migratory capacity was similar between different labeling conditions but slightly less efficient wound healing was observed after 28 h for 19F-labeled CBG99 (17.2% ± 2.2% wound size) compared to CBG99 19F-unlabeled cells (9.9% ± 3.0%, Fig. 1E, *t*-test, $t(7) = -3.667$, $p = 0.008$). In order to study the long-term effect of the different labels and their combination, we performed a more sensitive enzyme assay of cell viability and measured CBG99 mRNA levels up to 2 weeks – a similar time scale we later used for *in vivo* experiments (Fig. 1F + G). Shortly after labeling, cell viability was decreased for 19F-labeled, CTO labeled, and multi-labeled CBG99 cells compared to unlabeled controls (one-way ANOVA, $F(3,20) = 163.412$, $p < 0.001$, Bonferroni corrected post hoc $p < 0.001$ for all). 7 days later, a significant effect was only found for 19F ($p < 0.001$) and CTO ($p = 0.004$) whereas long-term viability at 14 days was again influenced by all labeling strategies (19F: $p = 0.002$, CTO: $p < 0.001$, multi-label: $p < 0.001$). CBG99 mRNA levels in single-labeled (19F or CTO) or multi-labeled transgenic NSCs were not altered except for a decrease at 14 days for the multi-labeled by a factor 0.292 (s.e. range 0.189–0.465, REST calculation). The differentiation capacity into neurons and glia was not significantly affected (Fig. 1H + I). However, qualitative PCR data for 19F-labeled CBG99 cells indicates a weaker GFAP, DCX and betaIII tubulin expression compared to 19F-labeled WT cells (Fig. S1A). In summary, the multi-labeling and luciferase expression had a number of transient and few long-term effects on NSCs *in vitro*.

3.2. Multimodal in vivo imaging of implanted NSCs

We tested specificity and detection sensitivity of *in vivo* 19F-MRI and BLI in a proof-of-concept study. Grafts of 300,000 19F-labeled NSCs were implanted in the striatum or s.c. in the neck of a naïve mouse. All grafts were detectable on 19F MR images, however, with ~5 times lower SNR for the striatal implant compared to the s.c. implant due to larger distance from the radiofrequency coil. BLI revealed signal from transgenic NSCs well above background signal from a WT control graft. BLI signal from the deeper implant in the striatum was ~10 times lower compared to the s.c. implant due to limited light tissue penetration depth (Fig. S2).

All provided *ex vivo* and *in vivo* reporter systems including histological validation of graft localization are summarized in Fig. 2.

NSC graft localization, density and survival in naïve and stroke-damaged brain Depots of 300,000 NSCs were implanted in the striatum of healthy mice ($n = 5$) or in the peri-infarct zone of mice that had undergone MCAO 48 h before ($n = 4$). BLI signal, thus the fraction of viable cells, dropped over 4 weeks down to 22% ± 18% of the first measurement at one week after implantation in naïve mice. Notably, a similar dramatic drop down to 27% ± 12% was observed in stroke animals (Fig. 3A). The main effect of time was highly significant (mixed model repeated measures ANOVA, $F(3,21) = 99.409$, $p < 0.001$) whereas no significant differences were detectable between naïve and stroke groups ($F(1,7) = 0.002$, $p = 0.969$). In contrast, 19F-MRI signal, a measure of cell density, did not show a corresponding temporal decrease (Fig. 3B). No main effect of time could be detected (mixed model repeated measures ANOVA $F(3,21) = 1.707$, $p = 0.196$) and differences between stroke

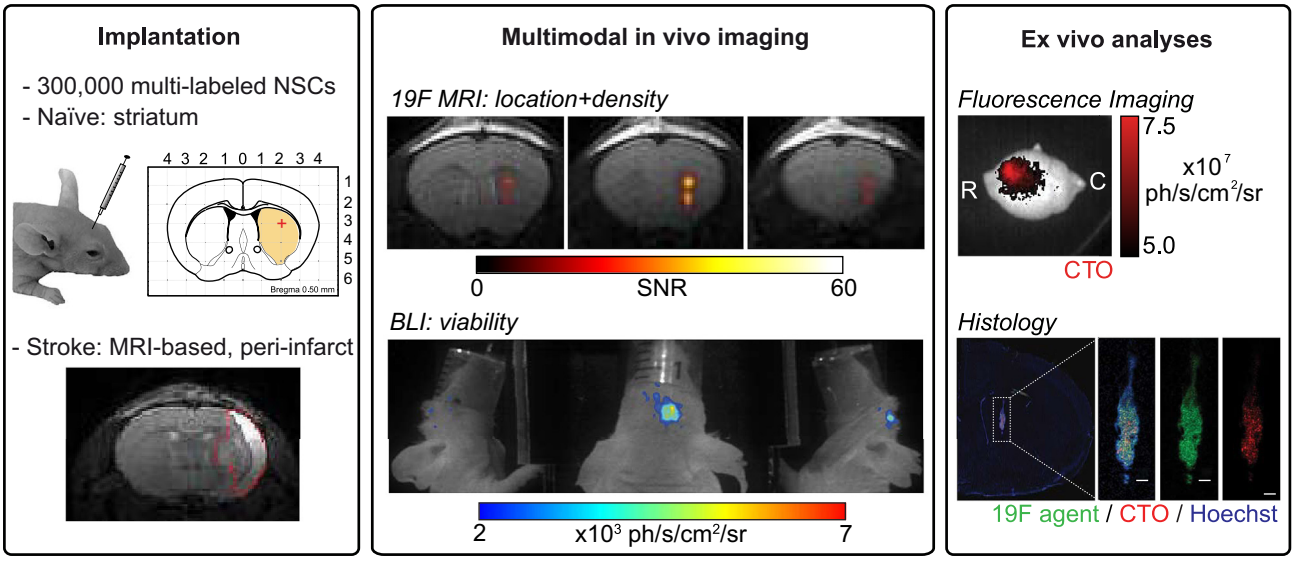

Fig. 2. Implantation procedure and reporters for *in vivo* imaging and *ex vivo* analyses. Left panel: 300,000 multi-labeled NSCs were implanted into the striatum of mice. Stereotactic coordinates are shown on an image from the mouse brain atlas [44]. Mice with focal cerebral ischemia were scanned with T2-weighted MRI 24 h after MCAO to delineate the lesion and to define coordinates for striatal, peri-infarct implantation at 48 h post stroke on an individual basis. Center panel: 19F-MRI provides localization of cells in 3D together with SNR as a measure of cell density. Three consecutive coronal slices through the brain are shown with 19F signal overlaid in false color (top). BLI signal intensity is a measure of cell graft viability. Top view and side views from two mirrors placed next to the animal are shown to better localize the origin of signal (bottom). Right panel: Cytosolic fluorescence marker CTO allows *ex vivo* fluorescence imaging of the graft on the excised brain (top view, R: rostral, C: caudal) for verification of *in vivo* imaging. A fluorescent 19F agent can be used to further discriminate NSCs from 19F label on histological sections by fluorescence microscopy (scale bar 200 nm). Images of center and right panel are of the same naïve animal, 24 h after implantation.

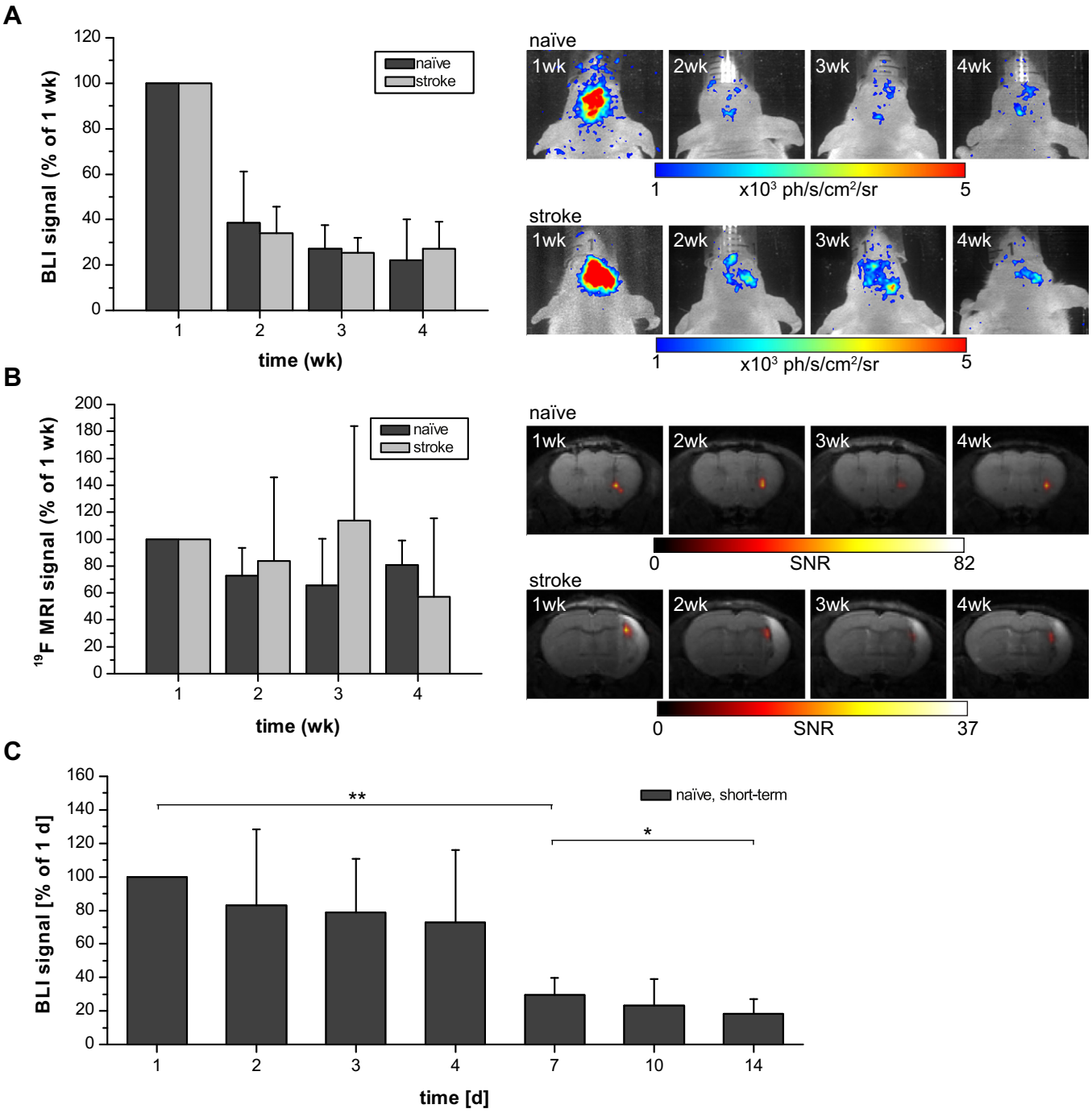

Fig. 3. Stem cell localization and viability after implantation. BLI and 19F-MRI signal after implantation into naïve mice and stroke animals that underwent MCAO 48 h before. (A) BLI signal in both naïve ($n = 5$) and stroke ($n = 4$) animals decreased rapidly over 4 weeks indicating impaired graft survival. (B) 19F SNR in naïve and stroke animals persisted with more scatter in the stroke group. (C) To better resolve the decrease in BLI signal, a separate group of naïve animals ($n = 6$) underwent BLI one day after implantation and up to 2 weeks after. The onset of decreased graft survival was found at 7 days. */**: Significance level $p \leq 0.05/0.01$, all values presented as mean ± standard deviation.

and naïve mice were not significant ($F(1,7) = 0.202$, $p = 0.667$). No NSC migration could be resolved by 19F MR images.

We attributed the persisting 19F-MRI signal to a limited clearance of the PFC when cells die and release the agent to the surrounding. In order to assess this clearance from the brain, we injected 2 μL of the undiluted PFC emulsion in the striatum of naïve mice ($n = 3$). Animals were imaged with 19F-MRI and sacrificed for histology at different time points. After four weeks, 55% of the initial 19F signal at 24 h was still detectable in the animal that survived the longest (Fig. S3).

To better resolve the temporal profile of graft survival in the early phase after implantation we implanted 300,000 NSCs in the striatum of naïve mice ($n = 12$). Animals were scanned repetitively with BLI on days 1–4, 7, 10, and 14 and sacrificed for histology after the last experiment ($n = 6$) or were sacrificed for histology already on days 4 ($n = 3$) and 7 ($n = 3$). To exclude any negative effect of the external labels (19F and/or CTO) on NSC viability, unlabeled CBG99 + NSCs were used. BLI signal remained stable within the first 4 days (Fig. 3C). More scatter was observed for the first measurements, which is likely due to healing of the implantation

wound that affects the light penetration properties of tissue. However, full closure of the wound and resolution of edema was observed in all animals latest at day 7. BLI signal, thus cell graft viability, was for the first time significantly reduced at 7 days after implantation (repeated measures ANOVA, main effect of time $F(6,30) = 15{,}284$ $p < 0.001$, Bonferroni corrected posthoc comparison of 7 days to 1 day, $p < 0.001$) and further decreased for the 14 day time point (Bonferroni corrected posthoc comparison to 7 days, $p = 0.023$).

3.3. Immunohistochemistry

NSC grafts were qualitatively investigated for the number of Nestin positive cells in the graft, cell proliferation, glial scar formation upon transplantation and immune response. The temporal profile of BLI signal was correlated with histological findings in a series of naïve animals whereas a comparison of healthy and stroke animals was carried out at the 4 week time point (Fig. 4). Resembling the BLI signal decrease, the number of Nestin positive NSCs in the graft location decreased over time to a minimal number of cells detectable after 4 weeks (Fig. 4A). In naïve animals, cell division remained active in cells of the graft border zone until 14 days after transplantation as assessed by positive Ki67 staining. However, single dividing cells were still detectable 4 weeks post transplantation in the stroke group (Fig. 4B). No clear evidence of NSC differentiation was found, apart from a small number of Nestin/GFAP double positive cells at the graft border (data not shown). In naïve animals, the host reaction upon allograft transplantation became visible by an increased GFAP reactivity in astrocytes surrounding the transplantation canal. From day 7 on, the reactive astrocytes started to form a dense glial scar shielding the graft from the host tissue. Strong GFAP reactivity around the needle tract was also found in a control group of naïve animals 7 days after saline implantation (data not shown). In contrast to the healthy group, astrocyte reaction in the stroke group remained spread widely on the complete hemisphere ipsilateral to the infarct without a corresponding glial scar formation (Fig. 4C). The temporal pattern of immune reaction in healthy animals was similar to that of GFAP reactivity. Iba1 staining for microglia and macrophages showed an accumulation of immune cells surrounding the NSC graft from day 7 on. Immune reaction in stroke animals was much more pronounced. In both healthy and stroke animals, colocalization of intracellular graft label CTO with Iba1 indicated phagocytosis of grafted cells by microglia/macrophages (Fig. 4D). In agreement with 19F-MRI data, no migration was detected, even in the context of stroke, despite a characteristic distribution of cells in the transplantation tract and the adjacent corpus callosum.

4. Discussion

Using a combination of 19F-MRI and optical imaging, this study investigates NSC viability in a living brain that underwent focal cerebral ischemia compared to healthy one. Our data demonstrate that graft survival is heavily impaired independent of this tissue status. Noninvasive imaging identified a critical time point of ~7 days for the onset of graft rejection. A pivotal role of the innate immune system in this process is suggested since mice deficient in the adaptive immune system were used and the imaging markers correlated well with microglial and astrocytic response.

Despite the use of non-phagocytic NSCs, efficient labeling with both 19F and fluorescent label CTO is possible without the help of transfection agents. Expression levels of CBG99 in genetically engineered NSCs are sufficient for BLI detection in deep tissue. In general, few effects of external and genetic labels on cell function were seen. However, an effect of 19F labeling on migratory and proliferation capacity was found and more sensitive enzymatic tests and qPCR revealed long-term effects in culture. These results are not surprising considering more recent literature on adverse effects of SPIO-based MRI labels on stem cells [26,27]. Expectedly, for SPIOs these effects were concentration dependent and similarly, a more detailed optimization of intracellular 19F doses in terms of cell MR-detectability and functionality is pending. Since the first 19F-MRI labels are entering the clinic in the context of cancer vaccines using dendritic cell implantations (press release, April 11 2013, Celsense Inc., Pittsburgh, USA), broader studies on possible adverse effects on cell function are urgently needed. In agreement with previous studies on stem cells [5–7,28,29], we found extremely low toxicity of PFCs *in vitro* considering the high payload of PFC per cell. Genetic labels are the preferred choice since external labels can be released or remain in tissue when cells die and in consequence even be transferred to other cells in the surrounding [30]. Our data indicate that the use of a multi-labeling strategy is necessary in order to cross-validate and rightfully interpret results. CTO is a versatile fluorescent label [31,32] and in our hands much more sensitively detected on histological slices than genetic labels such as green fluorescent protein (data not shown). However, we found CTO in microglia around the graft after 4 weeks indicating phagocytosis of dead cells or released label. Without Iba-1 co-staining these microglia cells would falsely be identified as living cells of the graft. Furthermore, we detected remaining 19F-MRI signal after cell transplantation despite impaired graft survival. This is in agreement with a study on SPIO MRI labels, for which persisting image contrast could be found up to 93 days although the graft was rejected much earlier [9]. These challenges could be overcome by the use of MRI reporter genes such as ferritin or peptides detectable via chemical exchange saturation transfer. However, the sensitivity and specificity for *in vivo* stem cell tracking in the brain has yet to be shown [33,34]. Positron emission tomography of herpes simplex virus thymidine kinase expressing NSCs was recently used to verify function of the graft in stroke rats [35] but challenges include the need for extensive radiochemistry infrastructure. Alternatively, in small animals, luciferases are a versatile genetic label to track transplanted stem cells. We used the PGK promoter in order to avoid down-regulation of CBG99 luciferase expression upon NSC differentiation since this phenomenon is known for the broadly used cytomegalovirus promoter [36]. Sensitivity of BLI of intraparenchymal transplants can further be improved by the use of a cranial window [19] or by optimization of luciferin doses and anesthesia as we have shown recently [25]. Genetic luciferase labeling to monitor graft function is therefore an emerging modality in rodents. It is complementary to 3D visualization of the graft and its cell density using 19F-MRI and overcomes many of the problems of external labels. Along these lines, our study shows that 19F-MRI is extremely helpful in the control of transplantation procedures but BLI appears more suited for reliable, unambiguous long-term cell tracking. We never observed NSC migration in the present study, which is coherent with other implantation experiments in rodents [14,17,37,38]. This may mechanically be explained by formation of an astrocytic scar encapsulating the graft and thus preventing (long distance) cell migration. Cell locomotion was also absent in stroke animals where glial scarring was much less pronounced thus indicating the expected lack of migratory cues for NSCs as the graft had been placed already next to the lesion target zone. Although we chose the timing, cell numbers, and site of implantation based on previous reports [13] to optimize graft survival, NSC viability dramatically decreased after transplantation. The phenomenon was observed in a large number of studies [13,14,18,19,37,39] and multiple contributing factors are hypothesized. The transplantation procedure itself can damage host tissue and lead to scarring and blood–brain

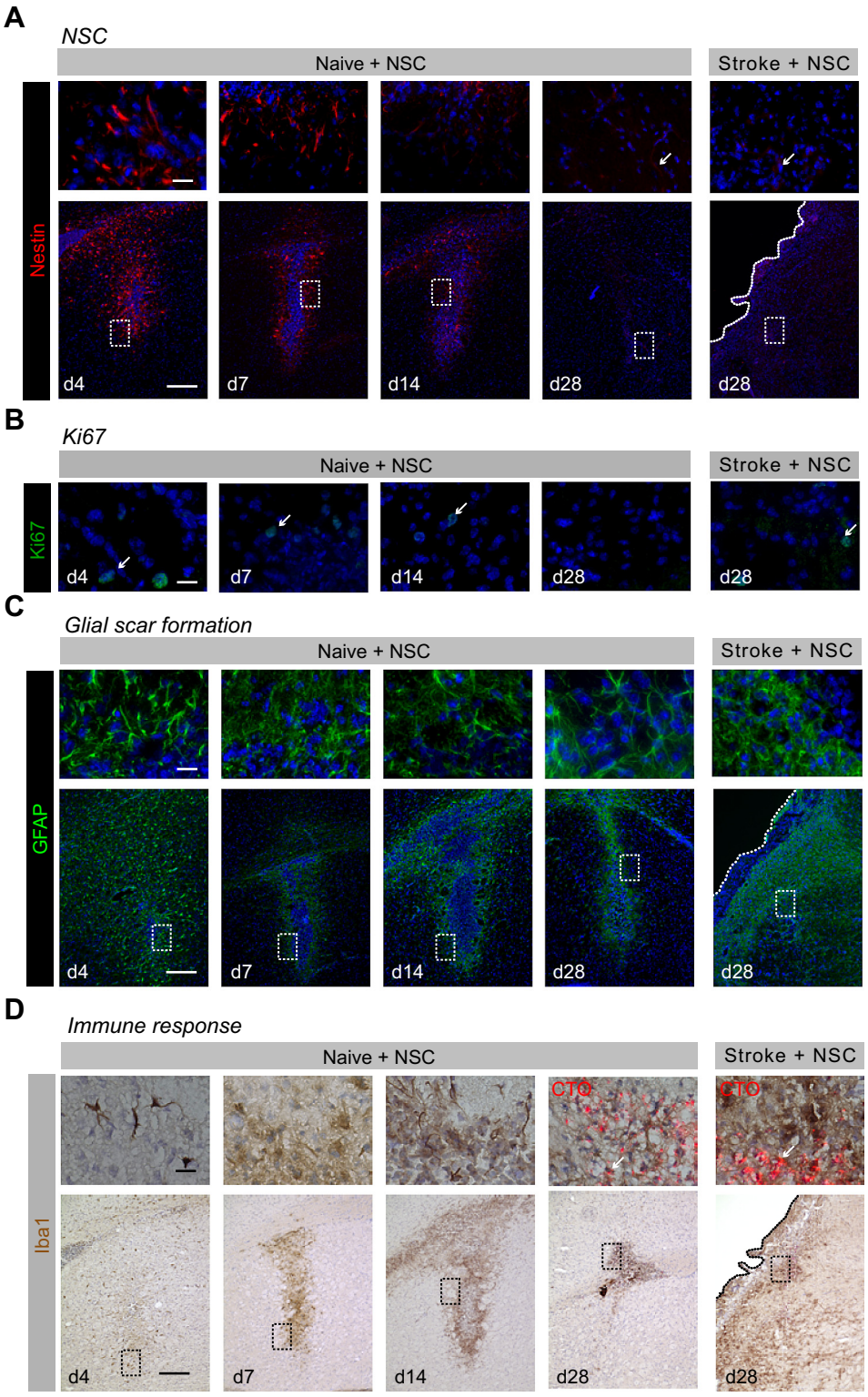

Fig. 4. Histological analysis of graft survival and host reaction in healthy and stroke mice. (A) The number of grafted cells expressing the NSC marker Nestin decreased strongly over time. Only single cells with weak Nestin reactivity were detected in both healthy and stroke tissue at day 28. (B) Proliferating cells were seen only in the first two weeks after transplantation in the healthy group, whereas single Ki67 positive cells were still detectable 4 weeks after transplantation in stroke mice. (C) Staining for GFAP revealed the reactivity of astrocytes triggered by transplantation and stroke. Glial scar formation around the transplantation canal occurred predominantly in naïve animals. (D) Innate immune reaction was visualized by staining for Iba1. Microglia and macrophage accumulation was detected from day 7 on with a larger extent in the stroke-affected hemisphere compared to naïve animals. At day 28, CTO was located in immune cells which indicated the phagocytosis of grafted cells or released labeling agents. Small images (60× magnification, scale bar 20 μm) correspond to white boxes in the graft border zone in larger images (10× magnification, scale bar 100 μm). Cell nuclei counterstained with Hoechst or Hematoxylin dye.

barrier breakdown although the latter did not correlate with cell graft survival in a recent study [17]. Along these lines we saw glial scarring in the brains of mice one week after sham saline implantations. When low infusion rates and thick needles are used, direct mechanical damage to grafted cells through shear stress is unlikely, which is supported by significant BLI signal up to 4 days in the present study and presence of NSCs of normal morphology on histological sections from one day after implantation. Within the first 24 h after transplantation, hypoxia, insufficient vascular support and lack of neurotrophic cues are believed to be the most significant contributors to cell death [40,41]. Since we imaged mice with BLI earliest at 24 h after implantation, cell death within this early time window could not be assessed. However, similarly to a previous study [41], an innate immune response started between day 4 and day 7 and correlated with a decrease in cell vitality as assessed by BLI. In agreement, the major fraction of host cells that contribute to graft rejection were shown to belong to the innate immune system whereas a considerably smaller fraction of cells of the adaptive immune system were found in another study [17]. Most importantly, our study indicates that innate immune reaction in response to the stroke does not further facilitate cell death compared to healthy tissue. Independent of these mechanistic aspects for the graft vitality, it is of note that this study answers an ongoing discussion whether a graft location adjacent to the ischemic territory may be considered sufficiently supportive for the graft survival. Our results show that cell survival in the peri-infarct zone is equivalent to that in the healthy hemisphere (comparable to the contralateral hemisphere in stroke animals).

5. Conclusion

NSCs bear hope to improve stroke tissue not only through cell replacement but also through release of trophic factors that can stimulate residing cells and neuroinflammation. However, a positive long-term effect is only to be expected when graft survival can be improved dramatically. Since the multiple factors that contribute to cell death follow different temporal profiles, only a fine-tuned combination of strategies such as the delivery of anti-apoptotic, neurotrophic or angiogenic compounds [42], enhanced structural support of cells using scaffolds [43], or suppression of the innate immune system through irradiation [37] may be successful. The multimodal imaging methods developed in this study will help to define relevant time points for interventions and to control their efficacy, also in contexts of cell therapy other than in stroke.

Acknowledgments

The authors thank Nadine Henn and Gabriele Schneider for excellent technical support, Laura Breucker and Annette Tennstädt for help with a pilot study and Stefan Wecker and Wilfried Haider for support with the MRI hardware setup. Generous supply of CS1000 green by C. O'Hanlon from Celsense Inc. is gratefully acknowledged. This work was financially supported by grants from the Volkswagen Foundation (I/83 443), the EU-FP7 program ENCITE (HEALTH-F5-2008-201842) and TargetBraIn (HEALTH-F2-2012-279017). The funding sources had no role in study design, in the collection, analysis and interpretation of data, in the writing of the report, and in the decision to submit the paper for publication.

Appendix A. Supplementary material

Supplementary material related to this article can be found at http://dx.doi.org/10.1016/j.biomaterials.2013.11.085.

References

[1] Oki K, Tatarishvili J, Wood J, Koch P, Wattananit S, Mine Y, et al. Human-induced pluripotent stem cells form functional neurons and improve recovery after grafting in stroke-damaged brain. Stem Cells 2012;30(6):1120–33.
[2] Bliss T, Guzman R, Daadi M, Steinberg GK. Cell transplantation therapy for stroke. Stroke 2007;38(2 Suppl.):817–26.
[3] Lindvall O, Kokaia Z. Stem cells in human neurodegenerative disorders – time for clinical translation? J Clin Invest 2010;120(1):29–40.
[4] Gera A, Steinberg GK, Guzman R. In vivo neural stem cell imaging: current modalities and future directions. Regen Med 2010;5(1):73–86.
[5] Bible E, Dell'acqua F, Solanky B, Balducci A, Crapo PM, Badylak SF, et al. Non-invasive imaging of transplanted human neural stem cells and ECM scaffold remodeling in the stroke-damaged rat brain by (19)F- and diffusion-MRI. Biomaterials 2012;33(10):2858–71.
[6] Boehm-Sturm P, Mengler L, Wecker S, Hoehn M, Kallur T. In vivo tracking of human neural stem cells with 19F magnetic resonance imaging. PLoS One 2011;6(12):e29040.
[7] Ruiz-Cabello J, Walczak P, Kedziorek DA, Chacko VP, Schmieder AH, Wickline SA, et al. In vivo "hot spot" MR imaging of neural stem cells using fluorinated nanoparticles. Magn Reson Med 2008;60(6):1506–11.
[8] Srinivas M, Heerschap A, Ahrens ET, Figdor CG, de Vries IJM. (19)F MRI for quantitative in vivo cell tracking. Trends Biotechnol 2010;28(7):363–70.
[9] Berman SC, Galpoththawela C, Gilad A, Bulte JWM, Walczak P. Long-term MR cell tracking of neural stem cells grafted in immunocompetent versus immunodeficient mice reveals distinct differences in contrast between live and dead cells. Magn Reson Med 2011;65(2):564–74.
[10] Daadi MM, Li Z, Arac A, Grueter B, Sofilos M, Malenka RC, et al. Molecular and magnetic resonance imaging of human embryonic stem cell-derived neural stem cell grafts in ischemic rat brain. Mol Ther 2009;17(7):1282–91.
[11] De Vocht N, Reekmans K, Bergwerf I, Praet J, Hoornaert C, Le Blon D, et al. Multimodal imaging of stem cell implantation in the central nervous system of mice. J Vis Exp 2012;64:e3906.
[12] Miloud T, Henrich C, Hämmerling GJ. Quantitative comparison of click beetle and firefly luciferases for in vivo bioluminescence imaging. J Biomed Opt 2011;12(5):054018.
[13] Darsalia V, Kallur T, Kokaia Z. Survival, migration and neuronal differentiation of human fetal striatal and cortical neural stem cells grafted in stroke-damaged rat striatum. Eur J Neurosci 2007;26(3):605–14.
[14] Kallur T, Farr TD, Böhm-Sturm P, Kokaia Z, Hoehn M. Spatio-temporal dynamics, differentiation and viability of human neural stem cells after implantation into neonatal rat brain. Eur J Neurosci 2011;34(3):382–93.
[15] Rota Nodari L, Ferrari D, Giani F, Bossi M, Rodriguez-Menendez V, Tredici G, et al. Long-term survival of human neural stem cells in the ischemic rat brain upon transient immunosuppression. PLoS One 2010;5(11):e14035.
[16] Darsalia V, Allison SJ, Cusulin C, Monni E, Kuzdas D, Kallur T, et al. Cell number and timing of transplantation determine survival of human neural stem cell grafts in stroke-damaged rat brain. J Cereb Blood Flow Metab 2011;31(1):235–42.
[17] Janowski M, Engels C, Gorelik M, Lyczek A, Bernard S, Bulte JW, et al. Survival of neural progenitors allografted into the CNS of immunocompetent recipients is highly dependent on transplantation site. Cell Transplant 2013. http://dx.doi.org/10.3727/096368912x661328, [Epub ahead].
[18] Bergwerf I, Tambuyzer B, De Vocht N, Reekmans K, Praet J, Daans J, et al. Recognition of cellular implants by the brains innate immune system. Immunol Cell Biol 2011;89(4):511–6.
[19] Kim D-E, Tsuji K, Kim YR, Mueller F-J, Eom H-S, Snyder EY, et al. Neural stem cell transplant survival in brains of mice: assessing the effect of immunity and ischemia by using real-time bioluminescent imaging. Radiology 2006;241(3):822–30.
[20] Ying Q-L, Smith AG. Defined conditions for neural commitment and differentiation. Methods Enzymol 2003;365:327–41.
[21] Conti L, Pollard SM, Gorba T, Reitano E, Toselli M, Biella G, et al. Niche-independent symmetrical self-renewal of a mammalian tissue stem cell. PLoS Biol 2005;3(9):e283.
[22] Carlotti F, Bazuine M, Kekarainen T, Seppen J, Pognonec P, Maassen JA, et al. Lentiviral vectors efficiently transduce quiescent mature 3T3-L1 adipocytes. Mol Ther 2004;9(2):209–17.
[23] Bahmani P, Schellenberger E, Klohs J, Steinbrink J, Cordell R, Zille M, et al. Visualization of cell death in mice with focal cerebral ischemia using fluorescent annexin A5, propidium iodide, and TUNEL staining. J Cereb blood flow Metab 2011;31(5):1311–20.
[24] Aswendt M, Gianolio E, Pariani G, Napolitano R, Fedeli F, Himmelreich U, et al. In vivo imaging of inhibitory, GABAergic neurons by MRI. Neuroimage 2012;62(3):1685–93.
[25] Aswendt M, Adamczak J, Couillard-Despres S, Hoehn M. Boosting bioluminescence neuroimaging: an optimized protocol for brain studies. Sensi SL, editor. PLoS One 2013;8(2):e55662.
[26] Cromer Berman SM, Kshitiz, Wang CJ, Orukari I, Levchenko A, Bulte JWM, et al. Cell motility of neural stem cells is reduced after SPIO-labeling, which is mitigated after exocytosis. Magn Reson Med 2013;69(1):255–62.
[27] Soenen SJH, Himmelreich U, Nuytten N, De Cuyper M. Cytotoxic effects of iron oxide nanoparticles and implications for safety in cell labelling. Biomaterials 2011;32(1):195–205.

[28] Partlow KC, Chen JJ, Brant JA, Neubauer AM, Meyerrose TE, Creer MH, et al. 19F magnetic resonance imaging for stem/progenitor cell tracking with multiple unique perfluorocarbon nanobeacons. FASEB J 2007;21(8):1647–54.
[29] Helfer BM, Balducci A, Sadeghi Z, O'Hanlon C, Hijaz A, Flask CA, et al. 19F MRI tracer preserves in vitro and in vivo properties of hematopoietic stem cells. Cell Transplant 2013;22(1):87–97.
[30] Li Z, Suzuki Y, Huang M, Cao F, Xie X, Connolly AJ, et al. Comparison of reporter gene and iron particle labeling for tracking fate of human embryonic stem cells and differentiated endothelial cells in living subjects. Stem Cells 2008;26(4):864–73.
[31] Mäkinen M, Joki T, Ylä-Outinen L, Skottman H, Narkilahti S, Aänismaa R. Fluorescent probes as a tool for cell population tracking in spontaneously active neural networks derived from human pluripotent stem cells. J Neurosci Methods 2013;215(1):88–96.
[32] Progatzky F, Dallman MJ, Lo Celso C. From seeing to believing: labelling strategies for in vivo cell-tracking experiments. Interface Focus 2013;3(3):20130001.
[33] Vandsburger MH, Radoul M, Cohen B, Neeman M. MRI reporter genes: applications for imaging of cell survival, proliferation, migration and differentiation. NMR Biomed 2013;26(7):872–84.
[34] Vande Velde G, Rangarajan JR, Toelen J, Dresselaers T, Ibrahimi a, Krylychkina O, et al. Evaluation of the specificity and sensitivity of ferritin as an MRI reporter gene in the mouse brain using lentiviral and adeno-associated viral vectors. Gene Ther 2011;18(6):594–605.
[35] Daadi MM, Hu S, Klausner J, Li Z, Sofilos M, Sun G, et al. Imaging neural stem cell graft-induced structural repair in stroke. Cell Transplant 2013;22(5):881–92.
[36] Wang R, Liang J, Jiang H, Qin L-J, Yang H-T. Promoter-dependent EGFP expression during embryonic stem cell propagation and differentiation. Stem Cells Dev 2008;17(2):279–89.
[37] Niranjan A, Fellows W, Stauffer W, Burton EA, Hong C-S, Lunsford LD, et al. Survival of transplanted neural progenitor cells enhanced by brain irradiation. J Neurosurg 2007;107(2):383–91.
[38] De Vocht N, Bergwerf I, Vanhoutte G, Daans J, De Visscher G, Chatterjee S, et al. Labeling of luciferase/eGFP-expressing bone marrow-derived stromal cells with fluorescent micron-sized iron oxide particles improves quantitative and qualitative multimodal imaging of cellular grafts in vivo. Mol Imaging Biol 2011;13(6):1133–45.
[39] Bakshi A, Keck C, Koshkin VS, LeBold DG, Siman R, Snyder EY, et al. Caspase-mediated cell death predominates following engraftment of neural progenitor cells into traumatically injured rat brain. Brain Res 2005;1065(1–2):8–19.
[40] Burns TC, Verfaillie CM, Low WC. Stem cells for ischemic brain injury: a critical review. J Comp Neurol 2009;515(1):125–44.
[41] Reekmans K, De Vocht N, Praet J, Fransen E, Le Blon D, Hoornaert C, et al. Spatiotemporal evolution of early innate immune responses triggered by neural stem cell grafting. Stem Cell Res Ther 2012;3(6):56.
[42] Sortwell CE. Strategies for the augmentation of grafted dopamine neuron survival. Front Biosci 2003;8:s522–32.
[43] Bible E, Chau DYS, Alexander MR, Price J, Shakesheff KM, Modo M. Attachment of stem cells to scaffold particles for intra-cerebral transplantation. Nat Protoc 2009;4(10):1440–53.
[44] Paxinos G, Franklin KBJ. The mouse brain in stereotactic coordinates. 2nd ed.; 2001.